Correlating transmission and local electronic structure in planar junctions: A tool for analyzing transport calculations

P. Bose,[1,*] P. Zahn,[2] I. Mertig,[1,2] and J. Henk[1]

[1]*Max-Planck-Institut für Mikrostrukturphysik, Weinberg 2, D-06120 Halle (Saale), Germany*

[2]*Institut für Physik, Martin-Luther-Universität Halle-Wittenberg, D-06099 Halle (Saale), Germany*

(Received 23 December 2010; revised manuscript received 4 March 2011; published 31 May 2011)

We propose to correlate transmittance maps and spectral-density maps of planar junctions, in order to analyze quantitatively and in detail spin-dependent transport calculations. Since spectral-density maps can be resolved with respect to atom, angular momentum, and spin, the resulting correlation coefficients provide strong evidence of, e. g., which layers or which orbitals determine the tunnel conductances. Our method can be used for transport calculations within the Landauer-Büttiker formalism. Its properties and features will be discussed by means of a pure bcc Fe(001) lead as well as an extensively studied Fe(001)/MgO/Fe(001) magnetic tunnel junction.

DOI: 10.1103/PhysRevB.83.174451 PACS number(s): 72.25.Mk, 73.22.−f, 73.40.Gk

I. MOTIVATION

Spin electronics—or spintronics for short—is one of the major topics in contemporary physics (see, for example, Refs. 1 and 2). With respect to both device applications and fundamental physics, planar junctions have been and are being investigated experimentally and theoretically with great effort. The spin-dependent transport properties of magnetic tunnel junctions show up as tunnel magnetoresistance (TMR), which is the change of the conductance upon reversal of the magnetization direction in one of the two electrodes.[3,4] Replacing the insulating barrier by a ferroelectric material, a tunnel electroresistance (TER) effect can be observed in addition. In this case, the conductance depends as well on the orientation of the electrical polarization in the ferroelectric material.[5]

In TMR experiments, the current that is flowing through a tunnel device is detected in dependence on external fields and device parameters (e.g., bias voltage and individual layer thicknesses). The current-voltage characteristics of tunnel devices are often interpreted within the Jullière model,[6] perhaps due to its simplicity. The validity of this model has been severely questioned[7] because it relates the TMR ratio exclusively to the spin polarization of the electrodes and, thus, neglects the interface and barrier regions completely. If the Jullière model were valid, the tunnel conductance would not depend on the interface material at all, in contrast to observations. In other words, the interface region is essential and has to be described in theory as well as possible.

From the preceding it is evident that a reliable description of transport in planar junctions must capture the essential properties on an atomistic level. Hence, present theoretical investigations of transport rely on sophisticated first-principles approaches to the electronic and magnetic structures.

Advanced first-principles approaches to transport allow a very detailed analysis of the electronic structure and the conductance. In particular, the probably most important question—which orbitals in which layer determine the transport properties—can be answered. However, the amount of output data that is produced by modern computer codes becomes often unmanageable for human beings. Therefore, one restricts oneself to representative subsets or converts the numerical data into manageable representations. For example, one puts the focus of the analysis on a single wave vector in the two-dimensional Brillouin zone (2BZ), typically to the 2BZ center.[8] By doing so, one should be aware that such a restriction could fail because considerable parts of the 2BZ may contribute to the conductance. Examples of data representations are transmittance and spectral-density maps in the 2BZ (introduced in Sec. I) which have become established analysis tools. They allow one, in principle, to answer the above question. Because they are compared visually, they leave space for speculation and interpretation; or phrased differently, they introduce ambiguity. Apparently, there is need for an improved analysis tool which allows the analysis of transport properties unequivocally and quantitatively, rather than ambiguously and qualitatively.

In this paper, we propose a quantitative analysis of transport properties which goes beyond the approaches sketched above. We propose to correlate transmittance and spectral-density maps. The resulting correlation coefficients provide strong evidence of, for example, which layers or which orbitals determine the tunnel conductances. Our method can be used for any computer code which relies on a Landauer-Büttiker-type approach, thus being applicable in most of the present-day transport calculations. Its properties will be discussed for two junctions exhibiting a planar geometry.

The paper is organized as follows. In Sec. II we introduce our approach for analyzing transport calculations. Section III gives a brief overview of our numerical approach. The correlation analysis is applied in Sec. IV to a pure Fe(001) lead (Sec. IV A) and to an Fe(001)/MgO/Fe(001) magnetic tunnel junction (MTJ) (Sec. IV B). Concluding remarks are given in Sec. V.

II. THEORETICAL ANALYSIS OF THE TUNNEL CONDUCTANCE

We consider a planar junction which consists of a left electrode $\mathcal{L}$, an interface region $\mathcal{I}$, and a right electrode $\mathcal{R}$. Due to the translational invariance parallel to the interface region, the Bloch states in the electrodes are indexed by the (in-plane) wave vector $\boldsymbol{k}_\parallel$ in the 2BZ; $\boldsymbol{k}_\parallel$ is conserved in the scattering process.

The bias voltage V opens an "energy window of transport"; the chemical potentials $\mu_{\mathcal{L}}$ and $\mu_{\mathcal{R}}$ of $\mathcal{L}$ and $\mathcal{R}$, respectively, differ by $eV = \mu_{\mathcal{L}} - \mu_{\mathcal{R}}$. Without loss of generality we consider the case $V > 0$, for which incoming occupied Bloch states in $\mathcal{L}$ can be transmitted into outgoing unoccupied Bloch states in $\mathcal{R}$.

According to Landauer and Büttiker,[9,10] the conductance C is given by

$$C(V) = \frac{e^2}{h} \int_{\mu_{\mathcal{R}}}^{\mu_{\mathcal{L}}} \int_{2\mathrm{BZ}} T^{\mathcal{L}\to\mathcal{R}}(V; E, \boldsymbol{k}_\parallel)\, d^2\boldsymbol{k}\, dE. \tag{1}$$

The wave-vector integral is over the 2BZ. The transmittance $T^{\mathcal{L}\to\mathcal{R}}(V; E, \boldsymbol{k}_\parallel)$ is the sum over the transmission probabilities of all incoming occupied states λ in $\mathcal{L}$ and outgoing unoccupied states ρ in $\mathcal{R}$. It is related to the scattering matrix S of the interface region by

$$T^{\mathcal{L}\to\mathcal{R}}(V; E, \boldsymbol{k}_\parallel) = \sum_{\lambda\rho} \left| S^{\mathcal{L}\to\mathcal{R}}_{\lambda\rho}(V; E, \boldsymbol{k}_\parallel) \right|^2. \tag{2}$$

This transmittance is a key quantity in the proposed analysis; it is conveniently displayed versus $\boldsymbol{k}_\parallel$ at fixed E and V, in so-called transmittance maps (T maps). Note that T can be regarded as a global quantity since it depends on the electronic structure of the entire junction, that is, both electrodes (incoming and outgoing Bloch states) and the interface region (scattering matrix).

The local electronic structure of the device is described in terms of the spectral density

$$N_\alpha(V; E, \boldsymbol{k}_\parallel) = -\frac{1}{\pi} \mathrm{Im\ Tr}\, G^+(V; E, \boldsymbol{k}_\parallel)\big|_\alpha. \tag{3}$$

α is a compound index which can comprise, for example, layer, atom, orbital, angular momentum, spin indices, or point-group representation. For a given division of the complete index space, the subsets of α are disjointed. The trace Tr_α of Green's function G^+ is restricted to the given α and, thus, allows a detailed analysis of the electronic structure. As for the transmittance, the spectral density is displayed in maps versus $\boldsymbol{k}_\parallel$ (N maps).

In previous publications we analyzed the conductance by relating pronounced features in a transmittance map to features in the associated spectral-density maps. If these features showed up in both the T map and an N_α map, we concluded that the chosen set α determined the transmittance in this (V, E) region. This way we could show that for Fe/Mn/vacuum/Fe junctions, the topmost Mn layer governs their TMR ratio.[11] However, for more complicated systems it turns out that the visual inspection of the maps becomes ambiguous, tedious, and not very reliable. As a consequence, we propose to correlate properly normalized T and N maps by means of a projection (inner product). This procedure results in a set of a few unambiguous numbers which allows us to determine rapidly the set of significant α indices.

For given energy E and bias voltage V we define the average value of a function $X(V; E, \boldsymbol{k}_\parallel)$ of the transmittance $T(V; E, \boldsymbol{k}_\parallel)$ and the spectral density $N_\alpha(V; E, \boldsymbol{k}_\parallel)$ as the average over the 2BZ,

$$A_X \equiv \frac{1}{\Omega_{2\mathrm{BZ}}} \int_{2\mathrm{BZ}} X(V; E, \boldsymbol{k}_\parallel)\, d^2\boldsymbol{k}, \tag{4}$$

where $\Omega_{2\mathrm{BZ}}$ is the area of the 2BZ.The correlation coefficient $c_\alpha(V; E)$ is then defined by

$$c_\alpha(V; E) \equiv \frac{A_{TN_\alpha}}{\sqrt{A_{T^2} A_{N_\alpha^2}}}. \tag{5}$$

This quantity can be interpreted as an inner product of the normalized $T(V; E, \boldsymbol{k}_\parallel)$ and $N_\alpha(V; E, \boldsymbol{k}_\parallel)$. Since the latter are semipositive for all $\boldsymbol{k}_\parallel$, $0 \leqslant c_\alpha(V; E) \leqslant 1$.

Note that $c_\alpha(V; E)$ is invariant with respect to scaling $T(V; E, \boldsymbol{k}_\parallel)$ and $N_\alpha(V; E, \boldsymbol{k}_\parallel)$ (explicitly $T(V; E, \boldsymbol{k}_\parallel) \to \tau T(V; E, \boldsymbol{k}_\parallel)$ and $N_\alpha(V; E, \boldsymbol{k}_\parallel) \to \nu N_\alpha(V; E, \boldsymbol{k}_\parallel)$). Further, for a visual inspection and comparison of the $X(V; E, \boldsymbol{k}_\parallel)$ on the same scale it is convenient to normalize them by

$$\widetilde{X}(V; E, \boldsymbol{k}_\parallel) \equiv \frac{X(V; E, \boldsymbol{k}_\parallel)}{\sqrt{A_{X^2}}}. \tag{6}$$

The correlation coefficient, alternatively expressible as $c_\alpha(V; E) = A_{\widetilde{T}\widetilde{N}_\alpha}$, is a measure of the "overlap" of T and N_α or of $\widetilde{T}$ and $\widetilde{N}_\alpha$. (i) Consider a constant transmittance and a constant spectral density, $T(V; E, \boldsymbol{k}_\parallel) = t$ and $N_\alpha(V; E, \boldsymbol{k}_\parallel) = n_\alpha$, which can be viewed as "completely overlapping." Then $A_{T^2} = t^2$, $A_{N_\alpha^2} = n_\alpha^2$, and $A_{TN_\alpha} = t n_\alpha$. Consequently, $c_\alpha = 1$, which we will consider as a perfect correlation. (ii) Consider a $T(V; E, \boldsymbol{k}_\parallel)$ which is nonzero only in a region Ω_T of the 2BZ:

$$T(V; E, \boldsymbol{k}_\parallel) = T(V; E, \boldsymbol{k}_\parallel) 1_{\Omega_T}(\boldsymbol{k}_\parallel), \tag{7}$$

with the indicator

$$1_{\Omega_T}(\boldsymbol{k}_\parallel) = \begin{cases} 1 & \boldsymbol{k}_\parallel \in \Omega_T, \\ 0 & \boldsymbol{k}_\parallel \notin \Omega_T. \end{cases} \tag{8}$$

Likewise, $N_\alpha(V; E, \boldsymbol{k}_\parallel)$ is assumed nonzero in a region Ω_{N_α} which is disjointed with Ω_T ($\Omega_T \cap \Omega_{N_\alpha} = \emptyset$; zero overlap). Consequently, $A_{T^2} \neq 0$, $A_{N_\alpha^2} \neq 0$, and $A_{TN_\alpha} = 0$, giving $c_\alpha = 0$. We consider this case as perfectly uncorrelated. We note in passing that there may be other definitions of correlation coefficients, as is the case for the correlation of random variables.[13]

The local partial density of states $\mathrm{PDOS}_\alpha = A_{N_\alpha}$ and the local density of states $\mathrm{LDOS} = \sum_\alpha A_{N_\alpha}$ ($\equiv A_{N_\Sigma}$) are computed based on N_α, respectively. With α summing up the elements of the orbital or alternatively the point-group index-space subsets, the LDOS represents in the following an atom-specific, site- and spin-dependent density of states.

A high partial density of states that coincides with a high transmission results in a large correlation, although the electronic states which produce the PDOS might not contribute to the transport. Therefore, it is important to note that consideration of a single correlation coefficient could possibly lead to a wrong conclusion, as will be clarified by the following example. Consider a transmission map with a maximum at the Brillouin zone center which is mainly due to spin-up states. Interface states lie in a bulk-band gap of the electrodes and thus do not contribute to the conductance in the Landauer-Büttiker approach. Hence, a spin-down majority

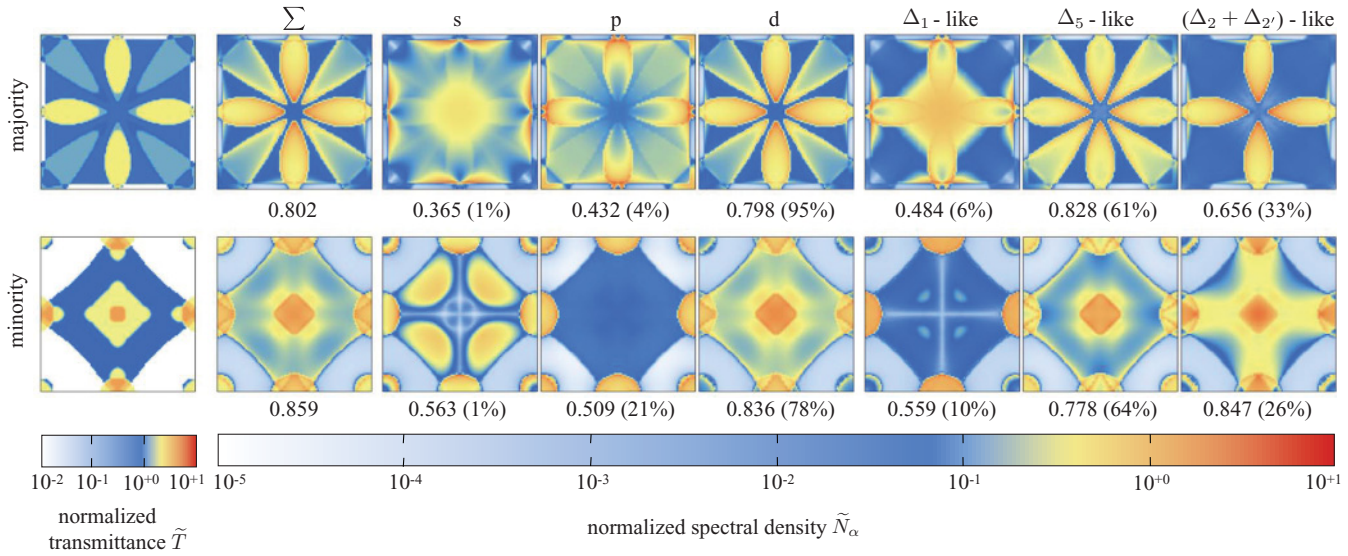

FIG. 1. (Color) Correlation analysis of the spin-dependent Sharvin conductance of Fe(001). Spin-resolved transmittance and spectral density maps are shown for the entire 2BZ (top row: majority channel; bottom row: minority channel). Each map is normalized according to Eq. (6). The $\widetilde{N}_\Sigma$ maps are decomposed with respect to the representations shown in Table I. The correlations c_α are given beneath each $\widetilde{N}_\alpha$ map. Numbers in brackets represent each map's partial contribution to the LDOS $\frac{A_{\widetilde{N}_\alpha}}{A_{\widetilde{N}_\Sigma}}$. Logarithmic color scales for $\widetilde{T}$ and $\widetilde{N}_\alpha$ are given at the bottom.

interface state located at the BZ center and in a spin-down bulk-band gap would result in both a high spin-integrated (L)DOS and correlation coefficient. But both the spin-up and the spin-down correlation coefficients would be small, indicating that this state does not contribute to the conductance. As a consequence, for our analyses (Secs. IV A and IV B), we have correlated transmission maps with different PDOSs (e.g., resolved with respect to spin, angular-momentum, and group-theoretical representation). The resulting entire set of correlations is then used to conclude on the relevant orbitals that determine the transport properties. However, there is still room for interpretation in our approach but considerably less than in other approaches.

III. CONDUCTANCE CALCULATIONS

Because our theoretical approach to spin-dependent tunneling has been described in detail elsewhere[11,14–17] we restrict ourselves to a brief survey here. The electronic structure of a tunnel junction is computed within the local spin-density approximation to density-functional theory, as is formulated in multiple-scattering theory.[18] Our spin-polarized relativistic layer Korringa-Kohn-Rostoker (KKR) method[19,20] provides on the one hand Green's function of the entire system, from which the spectral densities $N_\alpha(V;E,\boldsymbol{k}_\parallel)$ can be computed, Eq. (1). On the other hand, Green's function can be used to calculate the transmission $T(V;E,\boldsymbol{k}_\parallel)$, Eq. (2), within the framework of the Landauer-Büttiker theory.[21,22] We can also follow the approach introduced by MacLaren and Butler[23] in which the Bloch states in the electrodes and the scattering matrix of the interface region are computed by means of layer-KKR algorithms.[24] Here, Green's function is not computed explicitly.

The T and N maps have been computed on identical $\boldsymbol{k}_\parallel$ meshes in the entire 2BZ, with at least 40 000 points. In the following applications we restrict ourselves to the case of zero bias ($V = 0$ and $\mu_\mathcal{L} = \mu_\mathcal{R}$).

IV. APPLICATIONS

A. Fe(001)

The properties of the proposed correlation analysis are best introduced by an admittedly trivial case: the spin-resolved Sharvin conductance[25] of Fe(001). Because the three regions of the junction—$\mathcal{L}$, $\mathcal{I}$, and $\mathcal{R}$—are identical, the scattering matrix in Eq. (2) is $S_{\lambda\rho} = \delta_{\lambda\rho}$ and $T(\boldsymbol{k}_\parallel)$ is an integer. Accordingly, the N map is a projection of the Fermi surface onto the (001) plane. Without spin-orbit coupling, spin is a good quantum number; hence, we treat the majority and minority channels separately.

Figure 1 displays the normalized $\boldsymbol{k}_\parallel$-resolved transmittance and spectral-density maps. According to Table I, the latter

TABLE I. Decomposition α of the spectral density with respect to angular momentum (ℓ) and orbital (m) quantum numbers according to Eq. (3). Incrementing ℓ provides a classification by means of s, p, and d orbitals. An alternative decomposition can be obtained with respect to the irreducible representations of the point group C_{4v} [26]. Because such a decomposition holds strictly speaking only for the 2BZ center ($\overline{\Gamma}$, $\boldsymbol{k}_\parallel = 0$), we refer to "$\Delta_1$-like" maps, etc.

α	ℓ	m	Orbitals
Δ_1-like	0, 1, 2	0	s, p_z, $d_{3z^2-r^2}$
Δ_5-like	1, 2	−1, 1	p_x, p_y, d_{3xz}, d_{3yz}
Δ_2-like	2	−2	$d_{x^2-y^2}$
$\Delta_{2'}$-like	2	2	d_{3xy}

are ordered based on their $\{s,p,d\}$ or $\{\Delta_1,\Delta_5,\Delta_2+\Delta_{2'}\}$-like orbital contributions. The assignment of the angular-momentum orbitals to the different subsets α is motivated by the irreducible representations of the C_{4v} symmetry group. This decomposition is given in Table I.

(i) The map of the local spectral density $\widetilde{N}_\Sigma$ agrees nicely with the associated transmittance map in the majority channel (top row). In particular, all features are present and the correlation is consequently sizable ($c_\Sigma = 0.802$).

(ii) Other maps which essentially capture all features within the majority channel are the $\widetilde{N}_d$ and $\widetilde{N}_{\Delta_5-\text{like}}$ maps. A visual comparison of both with the transmittance could lead to the conclusion that the former matches slightly better than the latter. The correlation analysis, however, shows that this may be a misinterpretation; both coefficients indicate sizable correlations ($c_d = 0.798$ and $c_{\Delta_5-\text{like}} = 0.828$) but that of the Δ_5-like subset is slightly larger.

(iii) As a result of the relatively small correlation coefficients of s ($c_s = 0.365$) and p ($c_p = 0.432$) we identify the d majority states as the dominating conducting channels. Further, with the help of Table I and the c_α of the Δ-like maps, a hierarchy of conducting d states can be specified. Since $c_{\Delta_1-\text{like}} = 0.484$ is quite small, the $d_{3z^2-r^2}$ states seem to play no significant role. Due to the large $c_{\Delta_5-\text{like}}$ the d_{3xz} and d_{3yz} orbitals appear to form the leading transport channels, followed by the $d_{x^2-y^2}$ and d_{xy} states ($c_{(\Delta_2+\Delta_2')-\text{like}} = 0.656$).

(iv) Similar observations can be made for the minority channel (bottom row). Again, the d states represent the main conducting channels. But in comparison to the majority channel, the role of (d_{3xz}, d_{3yz}) and ($d_{x^2-y^2}$, d_{3xy}) orbitals is interchanged.

This example shows that the correlation analysis provides a powerful analysis tool which, on the one hand, fits nicely to the visual interpretation of T and N maps. On the other hand, it clearly reveals possible misinterpretations, as has become evident in point (ii).

With 95% (majority) and 78% (minority) the d states constitute by far the main contributions to the LDOS. In this example the hierarchy of correlation coefficients often reflects the hierarchy of partial contributions to the LDOS (see Fig. 1). This ordering becomes incorrect, for instance, in the case of Δ_5-like and $(\Delta_2+\Delta_{2'})$-like states in the minority channel. Here, the Δ_5-like states represent with 64% most of the LDOS, but exhibit with a $c_{\Delta_5-\text{like}}$ of 0.788 a smaller correlation than the $(\Delta_2+\Delta_{2'})$-like contributions (26%, $c_{\Delta_2+\Delta_{2'}} = 0.847$).

This last finding indicates already that a one-to-one mapping of PDOS hierarchies and correlation coefficients is not viable. In general, transmittances depend not only on the number of available states but rely also on other conditions like, e.g., the wave function matching at interfaces. Hence, as a prototype which exhibits more complicated correlations between transport and electronic structures properties, Fe/MgO/Fe MTJ will be discussed now.

B. Fe(001)/MgO/Fe(001)

In the following an Fe(001)/MgO/Fe(001) MTJ comprising six monolayers MgO is analyzed. The magnetic directions within both Fe leads are collinearly aligned to each other and considered for the case of a parallel magnetic configuration. Below we discuss the correlation analysis of the majority channel in more detail, because the current is dominated by the spin-up carriers.[8]

The corresponding transmittance map is displayed in Fig. 2. As is typical for $\widetilde{T}(\boldsymbol{k}_\parallel)$ in the majority channel [8], a Gaussian-like, radially symmetric distribution is found around the 2BZ center.

Let us suppose briefly that the Jullière[6] model is valid and that the transport properties can be interpreted exclusively based on the available PDOS$_\alpha$. Then the spin-polarized conductances are estimated with the product of the densities of states at the Fermi energy, strictly speaking with the PDOS$_\alpha$ inside the left ($\mathcal{L}$) and right ($\mathcal{R}$) leads. In this picture, the conducting channels would be, according to the previous discussion of iron, mainly determined by d-like or $\{\Delta_5,\Delta_2+\Delta_{2'}\}$-like Bloch states of the Fe electrodes. But a visual inspection and comparison with the majority maps in Fig. 1 reveals at first glance no similarity in the structures with either the $\widetilde{T}(\boldsymbol{k}_\parallel)$ or the $\widetilde{N}_d(\boldsymbol{k}_\parallel)$ maps.

Consequently, one could ask which states are essential for the transport processes if the predominant Fe bulk states do not play a decisive role. A closer look at the $\widetilde{N}_s$ and $\widetilde{N}_{\Delta_1-\text{like}}$ maps in Fig. 1 leads to the identification of centrosymmetric blobs like that in Fig. 2. But the associated Bloch states exhibit small c_α and marginal contributions to the LDOS in Fe bulk. Do these states play a decisive role for transport within the MTJ?

To answer this question we consider in a next step the layer-wise contributions of the PDOS$_\alpha$ to the respective LDOS at the Fermi energy (see Fig. 3). In particular, the $\frac{A_{\widetilde{N}_\alpha}}{A_{\widetilde{N}_\Sigma}}$ percentages are shown for one half of the symmetric MTJ and are classified again by means of $\{s,p,d\}$ or $\{\Delta_1,\Delta_5,\Delta_2+\Delta_{2'}\}$-like orbital decompositions.

The values for the outermost Fe layers in Figs. 3(a) and 3(b) are identical to those for the pure Fe lead in Fig. 1, indicating the bulk-like character of those layers far from the interfaces. The corresponding d states represent with 80%–95% the most numerous parts of the LDOS up to the second Fe layers adjacent to the MgO interfaces. At these interfaces the number of d states is drastically reduced. Within the MgO film the

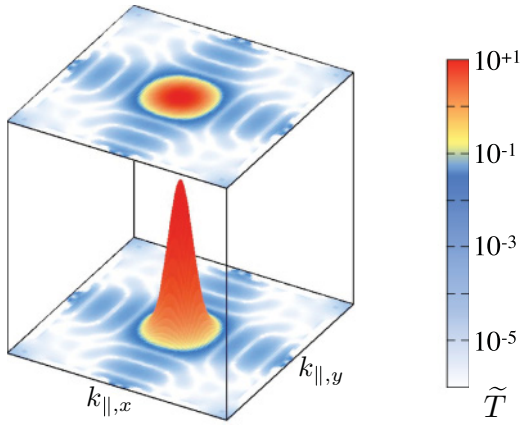

FIG. 2. (Color) Normalized majority transmittance map $\widetilde{T}(\boldsymbol{k}_\parallel)$ of an Fe(001)/6MgO/Fe(001) MTJ. The color scale for $\widetilde{T}$ is logarithmic.

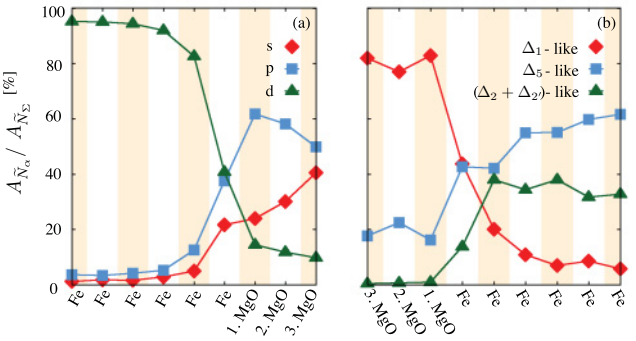

FIG. 3. (Color online) Layer- and orbital-resolved contributions of the local partial density of states $A_{\widetilde{N}_\alpha}$ to the local density of states $A_{\widetilde{N}_\Sigma}$ within the majority channel of an Fe(001)/6MgO/Fe(001) MTJ. The fractions are shown for (a) s, p, d, and (b) $\{\Delta_1, \Delta_5, \Delta_2 + \Delta_{2'}\}$-like orbital decompositions.

decrease is continued down to about 10% inside the middle region of the tunnel barrier.

On the other hand, the s and p contributions, which are apparently vanishingly small within the Fe electrodes, obtain substantial weight inside the MgO spacer. In particular, the p states exhibit a maximal percentage of 60% within the 1. MgO monolayer. Deeper inside the MgO, this fraction reduces to about 40%. In contrast, the s fractions reach a level of 20% at the Fe/MgO interfaces and increase monotonously to roughly about 40%. Thus, in the middle of the MgO the number of p and s states are comparably large, with a slight advantage of the former.

Further, a decomposition in $\{\Delta_1, \Delta_5, \Delta_2 + \Delta_{2'}\}$-like contributions reveals completely different characteristics in Fig. 3(b). Here, the Δ_1-like contributions, which are of minor importance within the Fe leads, experience a massive increase at the Fe/MgO interfaces and reach levels of about 80% within the tunnel barrier. The remaining 20% are predominantly occupied with Δ_5-like and a few $(\Delta_2 + \Delta_{2'})$-like states. This hierarchical order of PDOS$_\alpha$ within the MgO reflects the well-known fact of symmetry-selective decay lengths of the evanescent Bloch states within the tunnel barrier.[8,27]

Due to their sizable presence within the bottle neck of the junction, i.e., the MgO barrier, s and Δ_1-like states might indeed characterize the transport. But whether this predominance also results in a dominance of the conducting channels can only be answered by an analysis of the transmittance map in Fig. 2 with the respective $\widetilde{N}_\alpha$ maps. In order to specify exactly which layer-resolved spectral densities fit best the structures of the transmittance map, the $\widetilde{N}_\alpha$ maps of the whole Fe/MgO/Fe tunnel junction have to be inspected. These maps are shown in Fig. 4(a).

One can see immediately that $\widetilde{N}_\Sigma$, $\widetilde{N}_s$, $\widetilde{N}_p$, and $\widetilde{N}_{\Delta_1-\text{like}}$ within the MgO layers exhibit a great similarity with the structure of $\widetilde{T}(\boldsymbol{k}_\parallel)$ in Fig. 2. On the other hand, the similarities of $\widetilde{N}_d$, $\widetilde{N}_{\Delta_5-\text{like}}$ and $\widetilde{N}_{(\Delta_2+\Delta_{2'})-\text{like}}$ within the same layers appear rather small. Due to the great dissimilarities of the spectral-density maps within the Fe layers it is reasonable to expect low correlations there. But, based on visual comparisons, it is hard to make definitive statements about similarities of the structures and hence which states provide the largest contributions to the electronic transport of the whole MTJ.

At this point, the correlation analysis tool provides the potential to gain clearer statements. The computed correlation coefficients which represent a measure of the similarity of two maps are summarized in Figs. 4(b) and 4(c).

(i) Considering Figure 4(b), it turns out that s states exhibit the most prominent correlations in all layers. For each Fe layer, the c_s can be quantified with about 0.1–0.2 as nearly double as large as those of p and d states. Together with the significantly high correlations of 0.7 (1. MgO layer) up to 0.95 (3. MgO layer) inside the tunnel barrier, the previously assumed dominant role of the s states can be regarded as proven for the entire MTJ.

(ii) However, inside the MgO layers the p and d states exhibit sizable increases of their correlation coefficients, too. In particular, the c_p are with 0.2 (1. MgO layer), 0.4 (2. MgO layer) and 0.7 (3. MgO layer) approximately twice as high as the c_d. In the discussion of the $c_{\Delta_1-\text{like}}$ coefficients below, it will become evident that the increasing c_p and c_d are mainly related to states exhibiting p_z and $d_{3z^2-r^2}$ orbital character.

(iii) Since the LDOS maps comprise structures of s states closely correlated to the transmission map and less correlated p and d states, the correlation values of c_Σ are always lower than those for the s states.

(iv) Along the atomic layers of the MTJ, the characteristics of the $c_{\Delta_1-\text{like}}$ coefficients in Fig. 4(c) show a qualitatively similar dominance as was found for the c_s coefficients in Fig. 4(b). Within the Fe electrodes the correlations of the Δ_1-like states are just slightly but noticeably larger than those of the s states in these layers, indicating an additional relevance of p_z and $d_{3z^2-r^2}$ orbitals in the electronic transport. This finding is substantiated by relatively small correlations of both other Δ-like representations inside the tunnel barrier. Since the latter exhibit only $\{p_x, p_y, d_{3xz}, d_{3yz}\}$ and $\{d_{x^2-y^2}, d_{xy}\}$ orbital character (see Table I), it is reasonable to assume that the rising importance of p and d states inside the MgO is identical to an increasing significance of p_z and $d_{3z^2-r^2}$ orbitals.

The comparison of the results of the correlation analysis with the discussion of available PDOS$_\alpha$ in Fig. 3 shows common features but reveals also significant differences. A common outcome of both approaches is the principal importance of the tunnel barrier for the electronic transport of the MTJ. In particular, both discussions end up with a conclusion that Δ_1-like states— i.e., s, p_z, and $d_{3x^2-r^2}$ orbitals which are preferentially aligned along the transport direction—tunnel most effectively and consequently carry the dominant part of the tunnel current.

The fact that Δ_1-like states, especially those with s orbital character, show their decisive role also within the Fe leads represents a qualitatively different outcome of the correlation analysis. In contrast, these states exhibit the lowest PDOS$_\alpha$ contributions within the Fe layers in Fig. 3.

In principle, the symmetry-selective filtering of the MgO tunnel barrier shows up by means of the hierarchical order of the $\{\Delta_1, \Delta_5, \Delta_2 + \Delta_{2'}\}$-like PDOS$_\alpha$ fractions in Fig. 3. But deeper within the MgO these percentages stay rather constant. The layer-wise increase of the effective tunneling processes of Δ_1-like states inside the MgO can only be seen by the increasing characteristics of the $c_{\Delta_1-\text{like}}$ coefficients in Fig. 4(c).

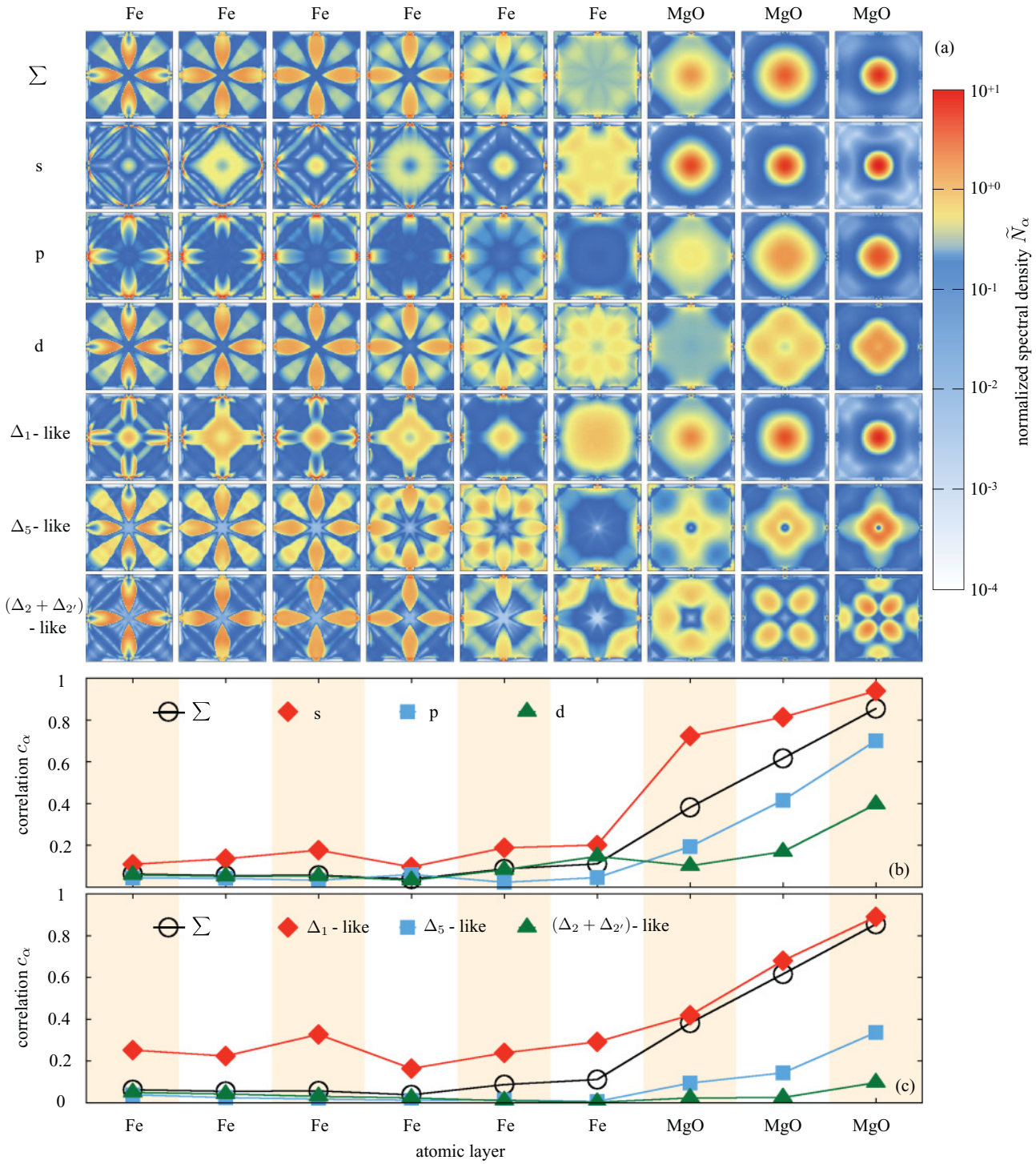

FIG. 4. (Color) Correlation analysis for the majority channel of an Fe(001)/6MgO/Fe(001) MTJ in parallel magnetic configuration. (a) Layer- and orbital-wise ordered spectral-density maps $\widetilde{N}_\alpha$ (left → right) are shown for the entire 2BZ with decompositions α according to Table I (top → bottom). Correlation coefficients c_α for contributions (a) with $\alpha = s, p, d$ and (b) $\alpha = \Delta_1$-like, Δ_5-like, $(\Delta_2 + \Delta_{2'})$-like. Color scales for $\widetilde{N}_\alpha$ are logarithmic.

V. CONCLUSIONS AND REMARKS

The analysis of transport properties within contacts that exhibit planar geometries is often accompanied with a visual comparison of large ensembles of $\boldsymbol{k}_\parallel$-resolved local spectral-density and transmission maps. In this article we presented an analysis tool which helps to avoid laborious inspections and potential misinterpretations by providing exact measures. Applying the proposed correlation analysis the contributions of atoms or orbitals can be quantified unambiguously. The dominance of the *s* states in the tunnel current of Fe/MgO/Fe MTJs could be proven even for the states in the Fe leads,

where the contribution of states to the LDOS is only marginal. Further, the method extends the popular discussion of transport properties at the $\bar{\Gamma}$ point in Fe/MgO/Fe MTJs to a more comprehensive analysis which comprises the entire 2BZ.

In principle, the proposed analysis technique is not restricted to planar junctions. For atomic-sized contacts, like point contacts or nanowires, there are of course no transmittance and spectral-density maps in reciprocal space, due to the lack of two-dimensional translational invariance. However, it is conceivable to relate local current-density maps perpendicular to the current flow with charge-density maps on the same planes in real space. Such a procedure could complete the physical insights as one would obtain from an analysis of the conduction eigenchannels.[28–30]

ACKNOWLEDGMENT

This work was supported by the DFG's Sonderforschungsbereich 762 "Functionality of Oxide Interfaces".

*pbose@mpi-halle.de

[1] D. Grundler, Phys. World **15**, 39 (2002).
[2] S. Wolf, D. Awschalom, R. Buhrman, J. Daughton, S. V. Molnar, M. Roukes, A. Chtchelkanova, and D. Treger, Science **294**, 1488 (2001).
[3] *Spin Dependent Transport in Magnetic Nanostructures*, edited by S. Maekawa and T. Shinjo (Taylor & Francis, London, 2002).
[4] I. Žutić, J. Fabian, and S. D. Sarma, Rev. Mod. Phys. **76**, 323 (2004).
[5] E. Tsymbal and H. Kohlstedt, Science **313**, 181 (2006).
[6] M. Julliere, Phys. Lett. A **54**, 225 (1975).
[7] J. M. MacLaren, X.-G. Zhang, and W. H. Butler, Phys. Rev. B **56**, 11827 (1997).
[8] W. Butler, X. G. Zhang, T. C. Schulthess, and J. M. MacLaren, Phys. Rev. B **63**, 054416 (2001).
[9] M. Büttiker, Y. Imry, R. Landauer, and S. Pinhas, Phys. Rev. B **31**, 6207 (1985).
[10] Y. Imry and R. Landauer, Rev. Mod. Phys. **71**, S306 (1999).
[11] P. Bose, I. Mertig, and J. Henk, Phys. Rev. B **75**, 100402 (2007).
[12] The considered area Ω has not necessarily to be extended over the whole 2BZ. Principally, Ω can be restricted to arbitrary parts of it.
[13] P. J. Bickel and K. A. Doksum, *Mathematical Statistics* (Holden Day, Oakland, CA, 1977).
[14] C. Tusche, H. Meyerheim, N. Jedrecy, G. Renaud, A. Ernst, J. Henk, P. Bruno, and J. Kirschner, Phys. Rev. Lett. **95**, 176101 (2005).
[15] P. Bose, A. Ernst, I. Mertig, and J. Henk, Phys. Rev. B **78**, 092403 (2008).
[16] M. N. Khan, J. Henk, and P. Bruno, J. Phys. Condens. Matter **20**, 155208 (2008).
[17] P. Bose, P. Zahn, J. Henk, and I. Mertig, Phys. Rev. B **82**, 014412 (2010).
[18] *Electron Scattering in Solid Matter*, edited by J. Zabloudil, R. Hammerling, L. Szunyogh, and P. Weinberger (Springer, Berlin, 2005).
[19] J. Henk, H. Mirhosseini, P. Bose, K. Saha, N. Fomynikh, T. Scheunemann, S. V. Halilov, E. Tamura, and R. Feder (unpublished).
[20] J. Henk, in *Handbook of Thin Film Materials*, edited by H. S. Nalwa, Vol. 2 (Academic, San Diego, 2002) Chap. 10, p. 479.
[21] J. Henk, A. Ernst, K. Saha, and P. Bruno, J. Phys. Condens. Matter **18**, 2601 (2006).
[22] K. K. Saha, J. Henk, A. Ernst, and P. Bruno, Phys. Rev. B **77**, 085427 (2008).
[23] J. M. MacLaren, X.-G. Zhang, W. H. Butler, and X. Wang, Phys. Rev. B **59**, 5470 (1999).
[24] J. M. MacLaren, S. Crampin, D. D. Vvedensky, and J. B. Pendry, Phys. Rev. B **40**, 12164 (1989).
[25] V. Sharvin, Sov. Phys. JETP **21**, 655 (1965).
[26] T. Inui, Y. Tanabe, and Y. Onodera, *Group Theory and Its Applications in Physics*, Springer Series in Solid State Sciences, Vol. 78 (Springer, Berlin, 1990).
[27] C. Heiliger, P. Zahn, and I. Mertig, Mater. Today **9**, 46 (2006).
[28] M. Brandbyge, M. R. Sørensen, and K. W. Jacobsen, Phys. Rev. B **56**, 14956 (1997).
[29] M. Paulsson and M. Brandbyge, Phys. Rev. B **76**, 115117 (2007).
[30] A. Bagrets, N. Papanikolaou, and I. Mertig, Phys. Rev. B **75**, 235448 (2007).